THE JOURNAL OF PHYSICAL CHEMISTRY B

ARTICLE

pubs.acs.org/JPCB

Vibrational Coherence from van der Waals Modes in the Native and Molten-Globule States of Zn^{II}-Substituted Cytochrome *c*

Kevin L. Dillman[†] and Warren F. Beck*

Department of Chemistry, Michigan State University, East Lansing, Michigan 48824, United States

ABSTRACT: The low-frequency vibrational coherence from Zn^{II}-substituted cytochrome *c* (ZnCytc) was characterized at room temperature in the native and acid/high-salt molten-globule states using femtosecond pump−probe, dynamic-absorption spectroscopy and impulsive excitation of the Soret absorption band. The pump−probe signals observed from the native state contain two types of modulation components in the vibrational coherence. The first type is a set of slowly damped (damping time $\gamma > 1.5$ ps) components with frequencies of 10, 30, 70, and 120 cm^{-1} that are assigned to out-of-plane vibrations of the porphyrin macrocycle following similar assignments in other porphyrin systems. A similar set of components is observed in the pump−probe signal from the molten-globule state, but the signal is much less strongly modulated. The second type is a strong, very rapidly damped ($\gamma < 150$ fs) 79 cm^{-1} modulation component that is assigned to van der Waals interactions between the porphyrin and nonpolar groups in its first solvation shell from the surrounding protein structure; the line shape and intensity of this component are comparable to those observed previously for bacteriochlorophyll *a* and Zn^{II} *meso*-tetrakis(*N*-methylpyridyl)porphyrin in solution. This component is almost completely absent from the signal from the molten-globule state. The results suggest that the van der Waals modes obtain intensity enhancement in the vibrational coherence because the attacking groups are displaced by the change of extent and/or change in shape of the π-electron density that accompanies the $\pi \rightarrow \pi^*$ optical transition of the Zn^{II} porphyrin. In the molten-globule state of ZnCytc, owing to the expanded hydrophobic core and to the loss of order for the groups that attack the π-electron density of the Zn^{II} porphyrin, the van der Waals modes are rendered effectively inactive. These results support an assignment of the broad low-frequency background in the spectrum of the vibrational coherence in purple bacterial photosynthetic reaction centers to van der Waals interactions between the primary electron donor, P, and the nonpolar protein-derived groups in its first solvation shell.

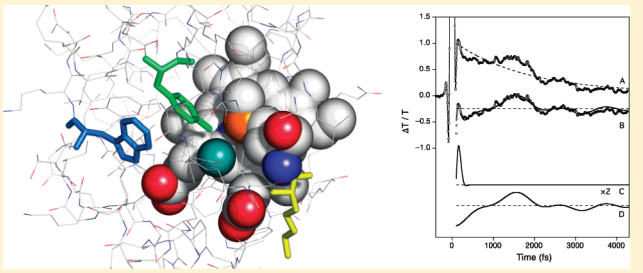

1. INTRODUCTION

The purple bacterial photosynthetic reaction center converts solar photons into a transmembrane chemical-potential gradient using two sequential charge-separation reactions that exhibit temperature-independent rates and essentially a 100% quantum yield.[1,2] How the protein structure's electrostatics[3] and internal motions[4] tune the reaction dynamics to obtain this level of quantum efficiency remains a significant question that is relevant to the design of artificial reaction centers or photocatalysts for fuel production. Central to this issue is the likelihood that certain vibrational motions of the protein render the forward, charge-separation reactions effectively irreversible by trapping the charged products that form on both sides of the membrane. The temperature independence of the primary electron-transfer reaction, from the bacteriochlorophyll dimer primary electron donor, P, to the bacteriopheophytin acceptor, $BPhe_L$, is attributed by Bixon and Jortner[5,6] to a near matching of the Gibbs free-energy change (the Marcus driving force) with the reorganization energy derived from vibrational modes from the protein medium in the 80−100 cm^{-1} range. The subsequent observations by Vos, Martin, and co-workers[7−15] of coherent wavepacket motion (or vibrational coherence) in femtosecond pump−probe, stimulated-emission transients from the lowest $\pi \rightarrow \pi^*$ excited state of P are consistent with the expectations of the Bixon and Jortner theory. A structural assignment for the active modes and the mechanism for their intensities in the vibrational coherence remain open questions that we consider further in this contribution.

There are at least two possible structural assignments for the low frequency of the vibrational modes that are coupled to electron-transfer reactions in the purple-bacterial reaction center. Vos and Martin assigned the modes that appear in the vibrational coherence from P to delocalized, phonon-like motions of the protein.[7,9,14] Such an explanation accounts for a low mode frequency with a large reduced mass for the coupled oscillators; a significant range of the protein medium encompassing the redox chromophores would be put in motion by an optical excitation of P and the subsequent long-distance electron transfer to $BPhe_L$. We have suggested as an alternative hypothesis that the low-frequency coupled modes arise from van der Waals interactions: from formally nonbonding interactions between the chromophores and groups in the first-solvation shell of the redox

Received: May 16, 2011
Published: June 01, 2011

dx.doi.org/10.1021/jp204571m | *J. Phys. Chem. B* 2011, 115, 8657–8666

chromophore.[16−19] These modes are especially well suited to modulate the electron-transfer dynamics and product yields in the reaction center. Because the van der Waals potential contains ion−dipole and ion−induced-dipole terms that are activated by the formation of charged products, the van der Waals modes trap the products of the charge-separation reactions in the peripheral, polar regions of the reaction center. Of critical importance to the yield of the secondary charge-separation reaction is the location of the bacteriopheophytin $BPhe_L$ intermediate in a nonpolar region of the structure. The activation energy required for the transfer of charge to the quinone acceptor is minimized by minimizing the charge-dependent terms in the intermolecular potential so that the rate of the forward electron-transfer reaction favorably competes with that of the reverse, charge-recombination reaction.[20]

The possible involvement of van der Waals modes in photosynthesis is raised by our observations of strong, solvent-dependent components in the vibrational coherence in polar solutions of bacteriochlorophyll *a* (BChl) and of Zn^{II} *meso*-tetrakis(*N*-methylpyridyl)porphyrin (ZnTMPyP). The mean frequency of these rapidly damped (damping time γ < 200 fs) modulation components exhibits a solvent dependence that follows the curving dipole-moment trend expected for the natural frequency of a van der Waals potential in which the London-dispersion and dipole−dipole terms make the largest contributions for neutral solutes.[17,19] In comparison to the components in the vibrational coherence arising from the skeletal (or intramolecular) normal modes of vibration of the chromophores in the <300 cm^{-1} regime, the intermolecular components are as much as an order of magnitude more intense.[16−20]

We focus in this contribution on the mechanism that couples the van der Waals modes to the electronic transition of a BChl or porphyrin chromophore in a folded protein so that their intensities are enhanced in the vibrational coherence. In polar solution, the solvent molecules in the first shell of the chromophore contribute most strongly to the vibrational coherence.[17,19] This conclusion is supported by our finding that the mode frequency in methanol solution of ZnTMPyP increases from 79 cm^{-1} in the ground state (S_0) to 256 cm^{-1} in the excited state (S_1). In the ground state, because the π-electron density is largely confined to the porphyrin macrocycle, the *coupled* solvents do not sense the charges; the ground-state intermolecular potential contains only charge-independent terms.[19] In the excited state, however, the π-electron density is extensively delocalized from the porphyrin to the peripheral *N*-methylpyridyl rings, each of which formally carries a positive charge. The excited-state intermolecular potential gains large terms from the ion−dipole and ion−induced-dipole interactions and exhibits an increased natural frequency.[20] These findings are consistent with the energetics of solvation in gas-phase chromophore−solvent clusters, where first-shell interactions account for a large fraction of the solvation reorganization energy (or Stokes shift).[21]

Our intention here is to test several of these ideas in a structurally well-characterized protein containing a single, intrinsic porphyrin chromophore. The best system of this type for our present purposes is Zn^{II}-substituted cytochrome *c* (ZnCytc)[22] because a partially unfolded state, the acid/high-salt molten globule,[23−25] is available for comparison to the normally folded (or native) state present under physiological solution conditions. The Zn^{II}-substituted and Fe^{II}-containing (Fe^{II}Cytc) cytochrome *c* proteins from horse heart have the same folded structures in solution, judging from their 2D NMR spectra,[26,27]

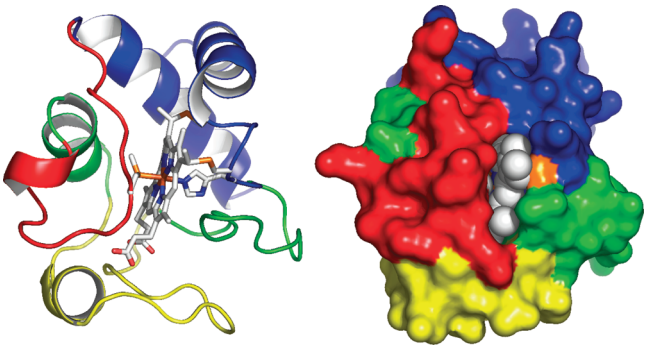

Figure 1. Ribbon (left) and surface (right) renderings of the X-ray crystal structure of horse-heart ferricytochrome *c* (1hrc.pdb).[44] The porphyrin, the methionine (M80), and histidine (H18) residues that serve as axial ligands to the Fe^{III} ion, and the cysteine residues (C14 and C17) that make thioether linkages to the porphyrin, are shown as stick representations in the ribbon picture and as space-filling spheres in the surface picture. The protein structure is color coded from red to blue in order of relative folding stability following the scheme of Englander and co-workers:[45] residues 70−85 (red), residues 36−61 (yellow), residues 20−35. and the α-helix over residues 60−70 (green), and the N- and C-terminal α helices (blue).

and it was possible to refine the structures of the Zn^{II} and Fe^{III} sites in Fe^{III}/Zn^{II} cocrystals of tuna-heart cytochrome *c* using starting coordinates derived from the X-ray crystal structure of the Fe^{III} protein (Fe^{III}Cytc) (Figure 1).[28,29] The molten-globule state of cytochrome *c* lacks the ordered protein−protein contacts that characterize the native tertiary structure, but most of the secondary structural content of the native state is retained.[23,25,30−37] The protein structure adopts an expanded configuration that rapidly samples a range of internal organizations; X-ray light-scattering experiments show that the Stokes radius of the cavity that surrounds the porphyrin in the molten-globule state is between 4 and 15% larger than that of the native state.[23,31] The Zn^{II} porphyrin in ZnCytc has proven useful to us in previous work as a fluorescent probe of the dynamics of the protein structure that surrounds it;[38−41] the absence of strong couplings to the low-lying porphyrin-to-metal or ligand-field states that quench the fluorescence in Fe porphyrins and lead to ligand photodissociation reactions[42,43] make ZnCytc a reasonable choice for a comparison to BChl-containing protein systems. We show here that the vibrational coherence obtained with Soret-band excitation of ZnCytc under native-state conditions contains a strong, very rapidly damped (γ < 150 fs) 79 cm^{-1} component that is fully consistent with an assignment to van der Waals interactions between the porphyrin and the essentially nonpolar environment provided in the first solvation shell by the surrounding folded protein. This component is almost completely absent in the signal from the molten-globule state owing to the expansion of the hydrophobic core and the loss of structural order of the surrounding protein groups that directly attack the Zn^{II}-porphyrin's π-electron density.

2. EXPERIMENTAL SECTION

Sample Preparation. ZnCytc was prepared from horse-heart Fe^{III}Cytc using the procedure developed in the Vanderkooi laboratory.[46] Liquid anhydrous hydrogen fluoride (Linde) was employed as the demetalating agent; the reaction was run on a home-built gas-handling system in Teflon reaction vessels. Metal

reconstitution of the free-base product with Zn^{II} was performed in the presence of a 10-fold molar excess of zinc acetate (Sigma 379786, 99.999%). The demetalated intermediate and Zn^{II}-reconstituted product solutions were worked up using ion-exchange chromatography following procedures derived from those of Winkler and co-workers[47] and Kostić and co-workers.[48] ZnCytc was equilibrated with a 25 mM sodium phosphate buffer solution at pH 6.9 by repeated concentration using an Amicon YM10 ultrafilter and dilution with the buffer solution. ZnCytc samples were stored at −78 °C as concentrated solutions in the pH 6.9, 25 mM sodium phosphate buffer solution.

Solutions of the acid-induced, high-salt molten-globule state of ZnCytc were prepared according to the methods developed by Goto and co-workers[30] and as described by Kostić and co-workers.[36] The molten-globule state is obtained by adjusting the pH of a ZnCytc solution prepared as described above to 2.0 with the addition of HCl and by adding solid NaCl to obtain a final concentration of 1.5 M.

For use in the femtosecond pump−probe experiments, solutions of ZnCytc in the native or molten-globule states were prepared by diluting the stock or acid-treated protein solutions to obtain an absorbance of 0.8 for a path length of 1.0 mm at the center of the laser spectrum at 420 nm for the native-state samples or at 418 nm for the molten-globule-state samples. The samples were held in the femtosecond pump−probe spectrometer at room temperature (23 °C) in a fused-silica flow cuvette (0.5 mm path length). A peristaltic pump was used to circulate a 10 mL reservoir of sample solution through the cuvette at 2.70 mL/min. The sample's absorption spectrum was monitored during the experiment for changes arising from photochemistry or permanent photobleaching. Fresh samples were prepared for each data-acquistion session; the reported signals represent the average obtained from several days of experiments.

Continuous-Wave Absorption and Fluorescence spectroscopy. Absorption spectra were obtained at 23 °C with a Hitachi U-2000 spectrophotometer (2 nm band-pass). Fluorescence spectra were acquired at 23 °C with a Hitachi F-4500 spectrofluorimeter (5 nm band-pass for the excitation and emission monochromators). As presented as a function of wavenumber, the fluorescence intensities are multiplied by the square of the wavelength in order to compensate for the fixed (in wavelength units) spectral band-pass of the emission spectrometer.[49]

Femtosecond Spectroscopy. Femtosecond pump−probe transients with impulsive excitation were recorded using the dynamic-absorption technique, in which the probe beam is dispersed in a grating monochromator after passing through the sample.[50−54] The present experiments were conducted with 50 fs pulses with intensity spectra centered at 420 nm for the native state and 418 nm for the molten-globule state (both 4 nm fwhm, as measured with an Ocean Optics USB-2000 spectrometer/CCD detector with a 0.5 nm band-pass), and a 1 nm band-pass of the transmitted probe beam detuned 2 nm to the red of the center of the laser spectrum, at about the half-maximum wavelength. This approach is similar to that used by Champion and co-workers in their studies of low-frequency vibrational coherence of heme proteins.[55−57]

The instrumentation and methodology used in these experiments is identical to that described in the previous work on ZnTMPyP.[19] The pump−probe spectrometer consists of a frequency-doubled, self-mode-locked Ti:sapphire oscillator (Coherent Mira-F oscillator and Verdi V5 (5 W) Nd:YVO_4 pump laser, Coherent/Inrad 5-050 second-harmonic generator), an SF10 Brewster prism−pair pulse compressor used prior to the frequency-doubling crystal, and a rapid-scanning, modified Mach−Zehnder interferometer with confocal sample and autocorrelation-crystal positions. The planes of linear polarization of the pump and probe beams were set to be 45° apart using calcite polarizers and $\lambda/2$-retarding wave plates. After passing through the sample, the probe beam was analyzed by another calcite polarizer oriented 90° relative to the pump-beam's plane of polarization, and then it was passed through a monochromator (Acton Research SP-150) on the way to an amplified photodiode (Thorlabs PDA55). The pump−probe signal was obtained from the photodiode signal using a lock-in amplifier (Femto LIA-MV-200-H); the pump beam was modulated at 100 kHz by a $\lambda/2$-retarding photoelastic modulator (Hinds Instrumentation) and a calcite polarizer.

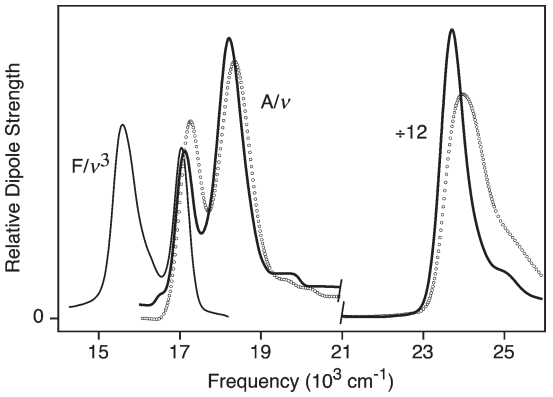

Figure 2. Soret ($\nu > 23\,000$ cm^{-1}) and Q-band regions of the continuous-wave absorption spectrum of ZnCytc in the native (solid curves) and molten-globule (circles) states. The fluorescence spectrum of the native state of ZnCytc at room temperature (23 °C) is shown overlapping and extending to the red of the absorption spectrum. The absorption spectra are approximately normalized to unit area with respect to the Soret bands; the fluorescence spectrum is scaled so that the intensity of the 0−0 vibronic transition matches that of the native-state Q band.

3. RESULTS

Figure 2 shows continuous-wave absorption and fluorescence spectra from the native state of ZnCytc at 23 °C. The spectra are plotted as relative dipole strengths[49,58,59] as a function of wavenumber ν, $A(\nu)/\nu$, and $F(\nu)/\nu^3$, respectively. The absorption spectrum features two bands, the Soret band and the Q band, in the blue and red parts of the spectrum, respectively. The fluorescence spectrum extends to the red from the 0−0 peak of the Q band. Also shown in Figure 2 is the absorption spectrum from the molten-globule state of ZnCytc. The absorption spectrum of the molten-globule sample is blue-shifted relative to that of the native state sample.

The dynamic-absorption transients we observed for the native and molten-globule states of ZnCytc are shown in Figures 3 and 4, respectively. Both signals exhibit an intense biphasic spike near the zero of time[60−62] that goes off the plotted scale on the positive pump-induced transmittance ($\Delta T/T$) side. The native-state transient (Figure 3) then exhibits a strong, very rapidly damped intensity modulation over the 100−600 fs delay range. The signal drops almost to the $\Delta T/T$ baseline at the positive delay side of the zero-time spike, and then it rises sharply to make a positive-going recurrence at the 170 fs delay point. The

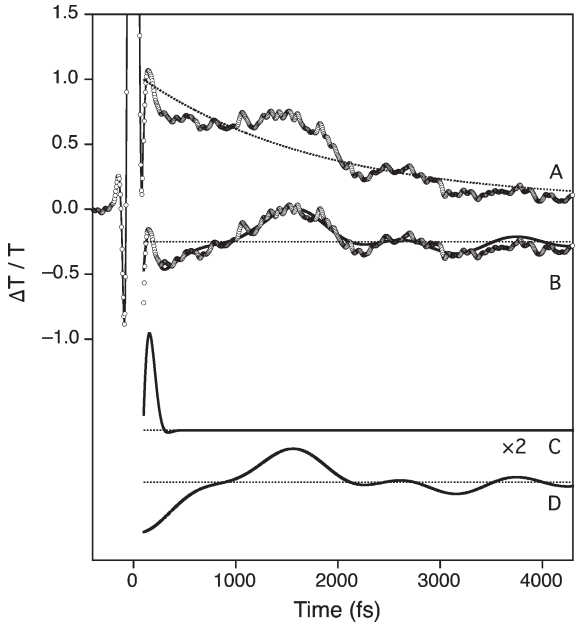

Figure 3. Femtosecond pump−probe transient from the native state of ZnCytc and fitted rapidly and slowly damped oscillatory model components. The transient was obtained with 50 fs, 420 nm pump and probe pulses and detected with a 1 nm band-pass of the transmitted probe spectrum centered at 422 nm. (A) Pump-induced change in transmission signal ($\Delta T/T$), shown superimposed on a single-exponential decay function (dashed curve) of the form $A_1 e^{-t/\tau_1} + A_0$, with $A_1 = 1.004$, $\tau_1 = 1.75$ ps, and $A_0 = 0.052$. The exponential decay is the best fit to the 100 fs−4.0 ps range of the $\Delta T/T$ signal. As plotted, the signal and exponential are normalized by dividing by the amplitude of the exponential at 100 fs. (B) Oscillatory residual, obtained by subtracting the fitted exponential function from the pump−probe transient. The data points are superimposed on a model for the residual containing both slowly and rapidly damped oscillatory components. The model parameters are listed in Table 1. (C) Rapidly damped ($\Delta\omega > 10$ cm^{-1}) part of the model. (D) Slowly damped ($\Delta\omega < 10$ cm^{-1}) part of the model. Trace C is shown with a 2× expanded ordinate compared to that for trace A, and the zero levels for traces B−D are marked by dashed lines.

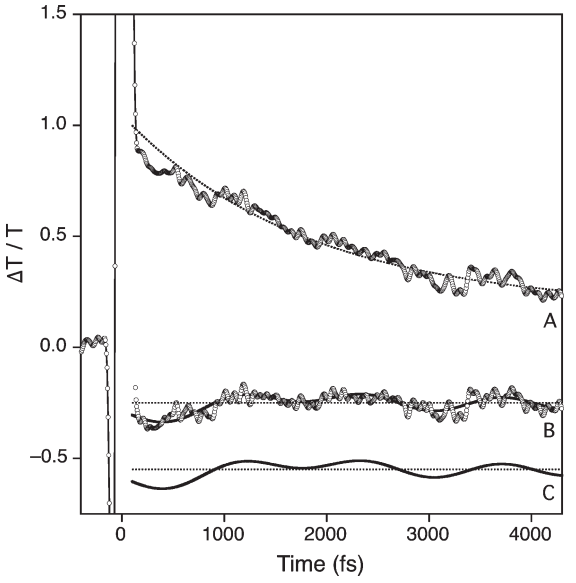

Figure 4. Femtosecond pump−probe transient from the molten-globule state of ZnCytc and fitted slowly damped oscillatory model components. The transient was obtained with 50 fs, 418 nm pump and probe pulses and detected with a 1 nm band-pass of the transmitted probe spectrum centered at 420 nm. (A) Pump-induced change in transmission signal ($\Delta T/T$), shown superimposed on a single-exponential decay function (dashed curve) of the form $A_1 e^{-t/\tau_1} + A_0$, with $A_1 = 0.873$, $\tau_1 = 1.78$ ps, and $A_0 = 0.175$. The exponential decay is the best fit to the 100 fs−4.0 ps range of the $\Delta T/T$ signal. As plotted, the signal and exponential are normalized by dividing by the amplitude of the exponential at 100 fs. (B) Oscillatory residual, obtained by subtracting the fitted exponential function from the pump−probe transient. The data points are superimposed on a model for the residual containing only slowly damped oscillatory components. The model parameters are listed in Table 2. (C) Model trace, for comparison to that in Figure 3. The zero levels for traces B and C are marked by dashed lines.

recurrence is followed by a rapidly damped oscillation that is largely damped at the ∼600 fs delay point. In contrast, the transient from the molten-globule sample (Figure 4) does not exhibit a strong modulation over the 100−600 fs delay range. The transition from the zero-time spike to the exponential decay that follows occurs at a net positive $\Delta T/T$ level, and there is no sign of a positive-going recurrence that is comparable to that in the native-state signal. Both transients then exhibit single-exponential decays that carry a pattern of slowly damped cosinusoidal modulations, the most intense of which have periods that are longer than 1 ps. The slowly damped modulations in the molten-globule signal are weaker by more than a factor of 5 than those in the native-state signal.

In order to obtain estimates for the line-shape parameters and relative intensities, the strongest modulation components in the pump−probe transients were modeled in the time domain using the approach we discussed previously.[19] Following truncation of the <100 fs portion,[62] the oscillatory part of the signal was isolated by subtracting a fitted ∼1.75 ps single-exponential decay function; the captions for Figures 3 and 4 list the model parameters for the native and molten-globule signals. The residual was then fit to the sum of oscillatory components of the form

$$I_i(t) = A_i e^{-t^2\sigma_i^2/2} \cos(\omega_{0i}t - \varphi_i)/\sqrt{2\pi} \quad (1)$$

with each component i having a center frequency ω_{0i} and phase φ_i. These waveforms correspond to Gaussian line shapes in the frequency domain

$$I_i(\omega) = A_i e^{-(\omega - \omega_{0i})^2/2\sigma_i^2}/(\sigma_i\sqrt{2\pi}) \quad (2)$$

where the line width is controlled by the standard deviation, $\sigma_i = \Delta\omega_i/2(2 \ln 2)^{1/2}$, and $\Delta\omega_i$ stands for the full width at half-maximum. Equations 1 and 2 are normalized so that the amplitude A_i corresponds to the area of the line shape in the frequency domain and to the intensity of the signal in the time domain.[19]

Model parameters for the slowly damped ($\gamma > 1.5$ ps, $\Delta\omega <$ 10 cm^{-1}) features were estimated initially from a Hanning-windowed (over the 100 fs−4 ps range) Fourier-transform magnitude spectrum (see Figure 5). The window function reduces truncation artifacts by damping the initial and final portions of the oscillatory signal to zero amplitude, so the rapidly damped, short-time part of the signal is strongly attenuated and line broadening is applied to the slowly damped components.[19] The Fourier-transform spectrum from both samples exhibits peaks at 10 and 27 cm^{-1} as the strongest features. The native-state spectrum also exhibits peaks at 72 and 120 cm^{-1} that are clearly above the noise; these probably correspond to peaks at 70 and 119 cm^{-1} in the

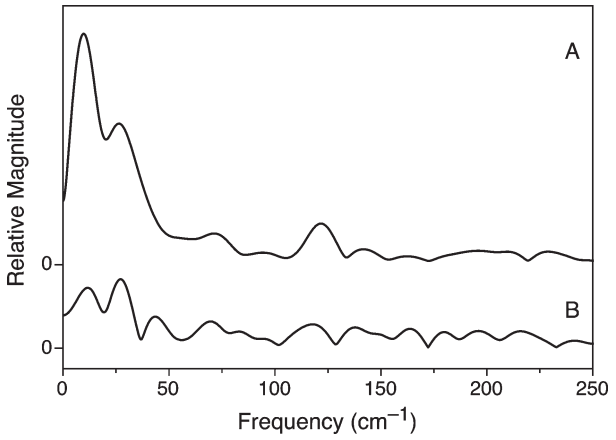

Figure 5. Hanning-windowed, Fourier-transform magnitude spectra of the oscillatory residuals (see traces B in Figures 3 and 4) from the femtosecond pump−probe transients observed for ZnCytc in the (A) native state and (B) the molten-globule state.

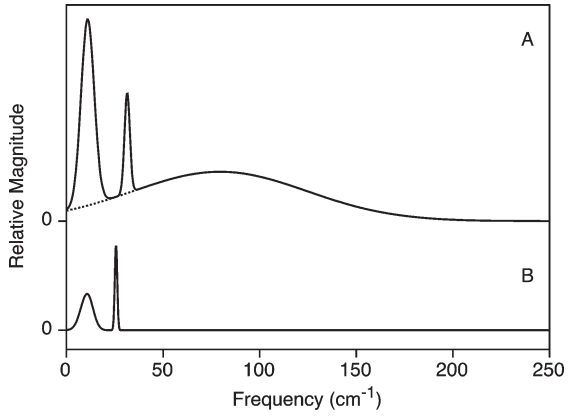

Figure 6. Frequency-domain representations of the fitted models for the oscillatory residuals (see traces B from Figures 3 and 4) from the femtosecond pump−probe transients observed for ZnCytc in the (A) native state and (B) the molten-globule state. The model parameters are listed in Tables 1 and 2, respectively.

Table 1. Gaussian Line-Shape Parameters for the Modulation Components Obtained from the Pump−Probe Transient from ZnCytc in the Native State (See Figure 3)

component	ω_0 (cm^{-1})	$\Delta\omega$ (cm^{-1})	amplitude[a]
1	10	8.02	0.809
2	31	3.25	0.177
3	79	106	2.84

[a] Relative to the normalized amplitude of the exponential decay of the pump−probe transient.

molten-globule spectrum, which has a much lower signal/noise ratio. Several of these mode frequencies are comparable to those observed by Champion and co-workers for vibrations of the porphyrin macrocycle that are mostly out-of-plane in character.[43,63] The relative weakness of the higher-frequency modulation components in both samples is consistent with the intermediate detuning of the probe band-pass from the center of the laser spectrum that was employed in these experiments.[57,64]

Table 2. Gaussian Line-Shape Parameters for the Modulation Components Obtained from the Pump−Probe Transient from ZnCytc in the Molten-Globule State (see Figure 4)

component	ω_0 (cm^{-1})	$\Delta\omega$ (cm^{-1})	amplitude[a]
1	11	7.76	0.157
2	26	0.575	7.08×10^{-2}

[a] Relative to the normalized amplitude of the exponential decay of the pump−probe transient.

Because of the limited signal/noise ratio, only the two strongest slowly damped components were included in the model.

Frequency-domain representations of the optimized time-domain models for the oscillatory parts of the native and molten-globule signals are shown in Figure 6. The parameters for these models are listed in Tables 1 and 2. The rapidly damped component in the native-state signal corresponds to the broad ($\Delta\omega$ = 106 cm^{-1}) line shape centered at 79 cm^{-1}. The intensity of this component is almost 4 times that of the 10 and 31 cm^{-1} components. The intensities of the 11 and 26 cm^{-1} slowly damped features in the model for the molten-globule signal are found to be 5 and 25 times smaller than the corresponding components in the native-state signal. Note that the oscillatory residual for the molten-globule signal (Figure 4B) exhibits a relatively weak rapidly decaying positive deviation from the fitted model in the 100−300 fs delay range that may correspond to the rapidly damped oscillatory signal observed in the native state. No attempt was made to model this part of the signal because its length is so short in the >100 fs region that was considered in the analysis, but it is obvious that its line shape would be very broad because of its especially rapid damping.

4. DISCUSSION

Just as we observed previously in polar solutions of BChl and ZnTMPyP, the modulation components in the vibrational coherence from ZnCytc with Soret-band excitation arise from two structurally distinct classes of vibrational modes that are displaced by the change in electronic structure associated with the $\pi \rightarrow \pi^*$ transition of the Zn^{II} porphyrin.[65,66] The structural origin of the two classes can be distinguished on the basis of their damping times or line widths. We assign the slowly damped components to out-of-plane motions of the Zn^{II} porphyrin macrocycle, and the rapidly damped component that appears only in the native-state signal is assigned to van der Waals modes between the Zn^{II} porphyrin and the groups from the surrounding folded protein that attack its π-electron density.

Both classes of modes obtain intensity enhancements in the low-frequency vibrational coherence on resonance with the Zn^{II} porphyrin's Soret band from the mode-specific gradients in the Franck−Condon region of the S_2-state potential-energy surface. The pump pulse in the dynamic absorption experiment sets wavepackets in motion on the ground-state (S_0) and S_2-state potential-energy surfaces along the coordinates of each of the coupled modes.[67−70] We assign the modulation components we observe in the pump−probe experiment predominantly to ground-state wavepacket motions in analogy to the assignment we made previously in ZnTMPyP.[19] The ~2 ps exponential decays that are observed in the pump−probe signals from ZnCytc in both the native and molten-globule states (see Figures 3 and 4) are very similar to those observed in ZnTMPyP solution, where they arise from vibrational cooling in the S_1-state

vibrational manifold following nonradiative decay of the S_2 state on the <100 fs time scale. The pump−probe signal's net ground-state depletion/stimulated-emission character decays because the blue shift of the broad $S_1 \rightarrow S_n$ excited-state absorption (ESA) spectrum that accompanies the vibrational relaxation process leads to a rising signal at the probe band-pass.[71] We assigned the vibrational coherence observed in ZnTMPyP to ground-state wavepacket motions because we considered it unlikely that the S_1-state population would retain the vibrational phase following the $S_2 \rightarrow S_1$ internal conversion.[19]

But if a nonradiative photophysical process occurs on a very short time scale, comparable to or shorter than that of the duration of the pump-pulse in a femtosecond pump−probe experiment (10−50 fs), vibrational coherence on the product state may be retained from that present initially or even produced by a curve-crossing event.[54,72] As one example, we recently reported that vibrational coherence is observed in solutions of the $Cr^{III}(acac)_3$ complex at room temperature due to coherent wavepacket motion on the ^2E surface after ultrafast intersystem crossing from the impulsively prepared $^4T_2$ state surface.[73] Further, in an example that is closer to the focus of the present contribution, coherent wavepacket motion on the lower of the two exciton states (P^*_-) of the primary electron donor, P, is observed in purple-bacterial reaction centers following interexciton-state nonradiative decay when the upper exciton state (P^*_+) is excited impulsively.[74,75] In these examples, the energy gap between the initial and final states linked by the nonradiative process is relatively small, so it is apparent that decoherence arising from intramolecular vibrational redistribution (IVR) occurs on a much longer time scale than the vibrational period for the coupled vibration. In contrast, because the energy gap for the $S_2 \rightarrow S_1$ internal conversion in Zn^{II} porphyrins is much larger, and accordingly the vibrational density of states in the product (S_1-state) vibrational manifold is very high, the IVR process would be expected to destroy the vibrational phase that is initially present on a much shorter time scale. For that reason, we consider an assignment of the vibrational coherence observed in the Soret band from ZnTMPyP and ZnCytc to ground-state wavepacket motions to be a more reliable assignment. This assignment must be considered provisional because we lack direct knowledge of the stimulated-emission spectrum of ZnCytc nor have we independently measured the $S_2 \rightarrow S_1$ internal-conversion time scale, which apparently depends sensitively in Zn^{II} porphyrins on the nature of the peripheral substitution of the porphyrin macrocycle.[71]

The slowly damped modulation features in the vibrational coherence from ZnCytc, observed in both folding states near 10 and 30 cm^{-1} and more weakly at 70 and 120 cm^{-1} (see Figure 5), exhibit relatively narrow line widths ($\Delta\omega$ < 10 cm^{-1}) and long damping times (γ > 1.5 ps). These features are consistent with out-of-plane motions of the Zn^{II} porphyrin chromophore in ZnCytc; analogous components are observed in ZnTMPyP but much less strongly in BChl.[16,17,19,20] The features at 30 and 70 cm^{-1} may correspond to metal-doming motions.[43] We suggest that these components appear much more strongly in the native state than they do in the molten-globule state because their intensities are enhanced by the out-of-plane distortions of the porphyrin macrocycle[76] that would be induced in the native fold by the imposition of a sixth ligand to the coordination field of the Zn^{II} ion, from the side chain of the methionine residue M80 that coordinates as an axial ligand in the native state of the $Fe^{II,III}$ protein.[28,44] A five-coordinate configuration with a single axial ligand for the Zn^{II} ion is favored in solution by Zn^{II} porphyrin complexes.[77−80] Six-coordinate Zn^{II} porphyrins are observed in crystals, but these structures are obviously strained by crystal-packing forces; the porphryin's pyrollic rings are canted out-of-plane so as to accommodate a larger core.[81−83] The frequencies of the core marker bands ν_3, ν_{10}, and ν_{19} observed by Kostić and co-workers in the resonance Raman spectrum from ZnCytc with Soret-band excitation[48] are probably better interpreted in terms of a strained six-coordinate structure than a five-coordinate structure.[38] In the molten-globule state, however, it is likely that the clamping forces applied by the M80 side chain are loosened as the hydrophobic core expands. This suggestion is consistent with the configuration observed in the molten-globule state of FeCytc, where M80 is replaced by a water molecule as an axial ligand to the Fe^{III} ion.[84] In the molten-globule state of ZnCytc, the Zn^{II} ion would be expected to retain only the axial ligation to the histidine (H18) ligand and assume a five-coordinate configuration.[34,36]

The line shape and relative strength of the strong, rapidly damped (γ < 150 fs) 79 cm^{-1} component that is observed only in the native state of ZnCytc are comparable to those of the solvent-dependent components we have discussed previously in BChl and ZnTMPyP solutions. That this component is effectively quenched in the molten-globule state shows that the coupling of the van der Waals modes to the π-electron density is remarkably sensitive to the expanded nonpolar cavity that surrounds the Zn^{II} porphyrin in the molten-globule state. The relatively low mean frequency and broad line shape is consistent with the general nature of the intermolecular potential for these modes and with the configuration of the native protein structure indicated by the X-ray crystal structure of Fe^{III}Cytc.

The frequency of the van der Waals modes can be qualitatively understood in terms of the solute−solvent intermolecular potential that was discussed in our earlier work on polar solutions of BChl and ZnTMPyP.[17,19] When there are no nearby charges present, the potential can be expressed as the sum of two terms: a repulsive, exchange term scaled by r^{-12} and a series of attractive terms scaled by r^{-6}

$$V_0(r) = a/r^{12} - \left(b\alpha_1\alpha_2 + \frac{c|\boldsymbol{\mu}_1|^2|\boldsymbol{\mu}_2|^2}{(4\pi\varepsilon_0)^2} + \frac{\alpha_2|\boldsymbol{\mu}_1|^2 + \alpha_1|\boldsymbol{\mu}_2|^2}{4\pi\varepsilon_0} \right) / D^2 r^6 \quad (3)$$

As shown previously,[17] a Taylor series expansion of eq 3 around the equilibrium geometry gives an expression for the natural frequency of the van der Waals mode

$$\nu = \frac{3}{(2a)^{2/3}} \left(b\alpha_1\alpha_2 + \frac{c|\boldsymbol{\mu}_1|^2|\boldsymbol{\mu}_2|^2}{(4\pi\varepsilon_0)^2} + \frac{\alpha_2|\boldsymbol{\mu}_1|^2 + \alpha_1|\boldsymbol{\mu}_2|^2}{4\pi\varepsilon_0} \right)^{7/6} / 2\pi D^{7/3} \mu^{1/2} \quad (4)$$

In these equations, r is the distance between the two molecules, $\boldsymbol{\mu}_i$ and α_i correspond to the dipole moment and polarizability of the chromophore solute and solvent (subscripts 1 and 2, respectively), μ is the reduced mass of the oscillator, D is the dielectric constant of the medium, and ε_0 is the permittivity of free space. The constant a scales the Pauli (exchange) interaction, b scales the London-dispersion interaction, $c = 2/3k_BT$ scales the dipole−dipole interactions, and the $\alpha_i|\boldsymbol{\mu}_j|^2$ terms correspond to dipole−induced-dipole interactions.[85−88] As expressed above, the dipole-moment-dependent terms apply to the high-temperature

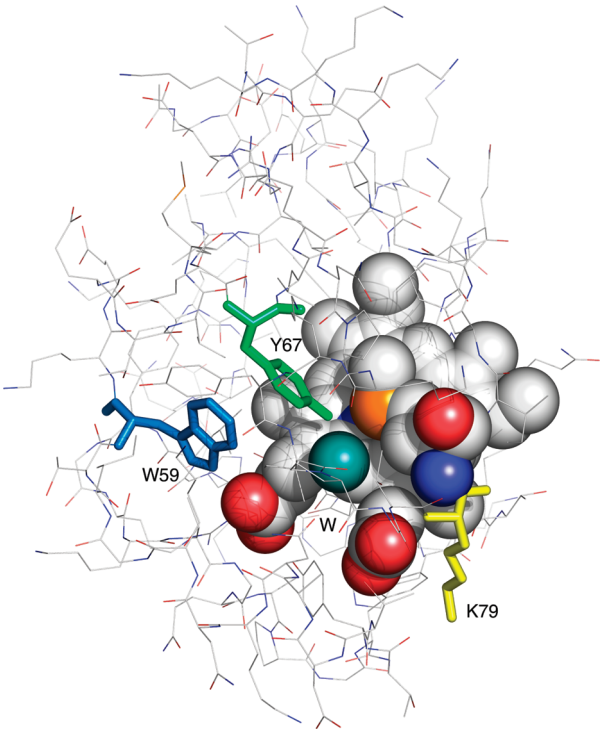

Figure 7. View of the X-ray crystal structure of horse-heart ferricytochrome *c* (1hrc.pdb)[44] depicting the packing of the protein around the porphyrin. The porphyrin and its axial ligands, from the side chains of M80 (front) and H18 (behind the porphyrin), and the oxygen atom from the conserved interior water molecule Wat-112 (W, blue-green, 3.77 Å) are rendered as space-filling (CPK) spheres. The polar amino acids W59 (blue, 5.29 Å), Y67 (green, 3.27 Å), and K79 (yellow, 6.79 Å) are rendered as stick structures. The distances are for the nearest-neighbor vector with respect to the porphyrin.

limit, where k_BT is much greater than the depth of the potential well, so the interactions are averaged over all orientations.[87] A further limitation is the use of the point-dipole approximation, which will not accurately describe the interaction of large chromophores like porphyrins with interacting solvent groups at short range. The potential nevertheless correctly describes the trend of the experimentally observed mode frequency on the dipole moment of the solvent in polar solutions of BChl and ZnTMPyP.[17,19]

When the solute or solvent has a charge $Q_{1,2}$, the attractive terms corresponding to the ion−dipole, ion−induced-dipole, and ion−ion interactions are added to the potential:

$$V_Q(r) = V_0 - \left(\frac{cQ_1|\boldsymbol{\mu}_2|^2 + cQ_2|\boldsymbol{\mu}_1|^2}{(4\pi\varepsilon_0)^2} + \frac{\alpha_2 Q_1{}^2 + \alpha_1 Q_2{}^2}{4\pi\varepsilon_0} \right) / 2D^2 r^4 + \frac{Q_1 Q_2}{4\pi\varepsilon_0 D^2 r} \quad (5)$$

This form of the potential is similar to that introduced previously[20] except that we now account for the charges that may be located either on the solute or solvent. The ion−dipole term depends linearly on the charge and the square of the dipole moment $\boldsymbol{\mu}_i$, and the ion−induced-dipole term depends on the polarizability α_i and exhibits a quadratic charge dependence. The Coulomb's law ion−ion term is linearly dependent on each of the charges $Q_{1,2}$. Additionally, the ion−dipole and ion−induced-dipole terms have an r^{-4} dependence on the solute−solvent distance, whereas the ion−ion term has an r^{-1} dependence. Thus, the charge-dependent terms cause the potential to extend to much greater distances than does the neutral potential. Equation 5 also predicts that the depth of the potential well increases significantly from that predicted from the neutral potential (eq 3), so the assumption of orientational averaging made for the uncharged case is no longer valid in solution, and the result would be an even more stable structure for the van der Waals complex. In a protein, the orientation of the solvent groups that surround the solute would be highly ordered by its connectivity to the polypeptide backbone and the steric environment derived from the packing of adjacent groups. Overall, the largest contributions to the van der Waals potential are those arising from the London-dispersion interactions and those involving nearby polar or charged residues.

The X-ray crystal structure of Fe^{III}Cytc (see Figure 7) indicates that the first-solvation shell of the porphyrin is provided by nonpolar groups. The nearest charged residue is a lysine residue (K79), but the ammonium ion is at least 6.79 Å from the porphyrin macrocycle. Aside from the axial ligands M80 and H18, the nearest polar groups in the surrounding protein medium are the side chains of the tyrosine and tryptophan residues, Y67 (3.27 Å) and W59 (5.29 Å). Polar interactions with nearby bulk water molecules can be neglected from consideration because the porphyrin is exposed only along the equatorial plane (see Figure 1). The conserved interior water molecule Wat-112 (Wat-166 in yeast *iso*-1-cytochrome *c*[89]), which is hydrogen bonded to the nearby N52, Y67, and T78 residues,[90] is 3.8 Å from the porphyrin. None of these groups is close enough to be considered effectively in contact with the porphyrin's π-electron density, so these groups will not be significantly displaced by the change in extent that accompanies the $\pi \rightarrow \pi^*$ transition. Thus, the coupled intermolecular modes that contribute to the vibrational coherence predominantly arise from nonpolar groups, and their interaction with the Zn^{II} porphyrin is accordingly mediated primarily by the London-dispersion term of the intermolecular potential. The line shape would be expected to be broad and inhomogeneous because all of the adjacent groups in the first solvation shell contribute to the interaction owing to their polarizabilities and each makes a distinct interaction strength. The trend of the mode frequency as a function of the solvent dipole moment obtained in the previous work on ZnTMPyP suggests a frequency in the nonpolar limit near 70 cm^{-1}.[19] The mean frequency and broad line shape (and rapid damping) of the 79 cm^{-1} component observed in the native state of ZnCytc is entirely consistent with these expectations.

The results from the present study, then, support the general hypothesis raised above that van der Waals interactions with first-solvation-shell groups from the surrounding molecular solvent or in a folded protein contribute strong, rapidly damped features to the vibrational coherence of BChl and Zn^{II} porphyrins. The mean frequency and line shape for the van der Waals modes in a protein should depend sensitively on the complement of groups that directly contact the chromophore's π-electron density. In the purple-bacterial photosynthetic reaction center, where the primary electron donor P is primarily solvated by nonpolar groups,[91,92] the spectrum from the vibrational coherence would be expected to exhibit an underlying broad line shape that is comparable to that presented here from ZnCytc in the native state with a mean frequency near 70 cm^{-1}. As we discussed previously in our study of the vibrational coherence from the paired BChl system in the B820 subunit from the LH1 light-harvesting complex,[18] the

mean mode frequency will be somewhat lower and the intensity enhancement in the vibrational coherence will be lessened by the extensive delocalization of the π-electron density over both of the BChl macrocycles in P.[93] Narrower line shapes, from the ordered direct interactions with dipolar or charged residues, will be superimposed on the broad background. This description is consistent with the changes in the spectrum resulting from point mutations on the vibrational coherence in *Rhodobacter sphaeroides* reaction centers, where polar and charged residues were introduced so as to alter hydrogen-bonding interactions between P and the surrounding protein structure.[14] The spectrum from each mutant is unique in having one or more relatively narrow peaks over a range of frequencies between ~50 and 150 cm^{-1}, but these varying sharp features are superimposed on a broad background line shape that is essentially independent of the mutation. Because the addition of polar or charged groups to the first solvation shell tunes the activation energy and enables trapping of the charged products for the forward, charge-separation reactions via short-ranged and rapidly damped displacements that mediate crossings from uncharged to charged intermolecular potentials,[20] we again suggest that the coupled van der Waals modes permit the surrounding protein structure to optimize the efficiency of the energy-storing electron-transfer reactions in photosynthesis compared to similar model systems in single-phased media.

AUTHOR INFORMATION

Corresponding Author

*E-mail: beck@chemistry.msu.edu.

Present Addresses

[†]Department of Chemistry, Colorado State University, Fort Collins, CO 80523.

ACKNOWLEDGMENT

This research was supported by the National Science Foundation Biomolecular Systems Cluster/Molecular Biophysics program under grants MCB-0520002 and MCB-0920101. We thank Jagnyaseni Tripathy for some helpful discussions concerning interpretation of the results.

REFERENCES

(1) Fleming, G. R.; Martin, J.-L.; Breton, J. Rates of primary electron transfer in photosynthetic reaction centers and their mechanistic implications. *Nature* **1988**, *333*, 190.

(2) Gunner, M. R.; Dutton, P. L. Temperature and $-\Delta G°$ dependence of the electron transfer from $BPh^{\bullet-}$ to Q_A in reaction center protein from *Rhodobacter sphaeroides* with different quinones as Q_A. *J. Am. Chem. Soc.* **1989**, *111*, 3400.

(3) Marchi, M.; Gehlen, J. N.; Chandler, D.; Newton, M. Diabatic surfaces and the pathway for primary electron transfer in a photosynthetic reaction center. *J. Am. Chem. Soc.* **1993**, *115*, 4178.

(4) Wang, H.; Lin, S.; Allen, J. P.; Williams, J. C.; Blankert, S.; Laser, C.; Woodbury, N. W. Protein dynamics control the kinetics of initial electron transfer in photosynthesis. *Science* **2007**, *316*, 747.

(5) Bixon, M.; Jortner, J. Coupling of protein modes to electron transfer in bacterial photosynthesis. *J. Phys. Chem.* **1986**, *90*, 3795.

(6) Bixon, M.; Jortner, J. Activationless and pseudoactivationless primary electron transfer in photosynthetic bacterial reaction centers. *Chem. Phys. Lett.* **1989**, *159*, 17.

(7) Vos, M. H.; Lambry, J.-C.; Robles, S. J.; Youvan, D. C.; Breton, J.; Martin, J.-L. Direct observation of vibrational coherence in bacterial reaction centers using femtosecond absorption spectroscopy. *Proc. Natl. Acad. Sci. U.S.A.* **1991**, *88*, 8885.

(8) Vos, M. H.; Lambry, J.-C.; Robles, S. J.; Youvan, D. C.; Breton, J.; Martin, J.-L. Femtosecond spectral evolution of the excited state of bacterial reaction centers at 10 K. *Proc. Natl. Acad. Sci. U.S.A.* **1992**, *89*, 613.

(9) Vos, M. H.; Rappaport, F.; Lambry, J.-C.; Breton, J.; Martin, J.-L. Visualization of the coherent nuclear motion in a membrane protein by femtosecond spectroscopy. *Nature* **1993**, *363*, 320.

(10) Vos, M. H.; Jones, M. R.; Hunter, C. N.; Breton, J.; Lambry, J.-C.; Martin, J.-L. Coherent dynamics during the primary electron-transfer reaction in membrane-bound reaction centers of *Rhodobacter sphaeroides*. *Biochemistry* **1994**, *33*, 6750.

(11) Vos, M. H.; Jones, M. R.; Hunter, C. N.; Breton, J.; Martin, J.-L. Coherent nuclear dynamics at room temperature in bacterial reaction centers. *Proc. Natl. Acad. Sci. U.S.A.* **1994**, *91*, 12701.

(12) Vos, M. H.; Jones, M. R.; Breton, J.; Lambry, J.-C.; Martin, J.-L. Vibrational dephasing of long- and short-lived primary donor states in mutant reaction centers of *Rhodobacter sphaeroides*. *Biochemistry* **1996**, *35*, 2687.

(13) Vos, M. H.; Jones, M. R.; Martin, J.-L. Vibrational coherence in bacterial reaction centers: spectroscopic characterisation of motions active during primary electron transfer. *Chem. Phys.* **1998**, *233*, 179.

(14) Rischel, C.; Spiedel, D.; Ridge, J. P.; Jones, M. R.; Breton, J.; Lambry, J.-C.; Martin, J.-L.; Vos, M. H. Low frequency vibrational modes in proteins: changes induced by point-mutations in the protein-cofactor matrix of bacterial reaction centers. *Proc. Natl. Acad. Sci.* **1998**, *95*, 12306.

(15) Vos, M. H.; Martin, J.-L. Femtosecond processes in proteins. *Biochim. Biophys. Acta* **1999**, *1411*, 1.

(16) Shelly, K. R.; Carson, E. A.; Beck, W. F. Vibrational coherence from the dipyridine complex of bacteriochlorophyll *a*: intramolecular modes in the 10−220 cm^{-1} regime, intermolecular solvent modes, and relevance to photosynthesis. *J. Am. Chem. Soc.* **2003**, *125*, 11810.

(17) Shelly, K. R.; Golovich, E. C.; Beck, W. F. Intermolecular vibrational coherence in bacteriochlorophyll *a* with clustered polar solvent molecules. *J. Phys. Chem. B* **2006**, *110*, 20586.

(18) Shelly, K. R.; Golovich, E. C.; Dillman, K. L.; Beck, W. F. Intermolecular vibrational coherence in the purple-bacterial light-harvesting proteins B777 and B820 from *Rhodospirillum rubrum*. *J. Phys. Chem. B* **2008**, *112*, 1299.

(19) Dillman, K. L.; Shelly, K. R.; Beck, W. F. Vibrational coherence in polar solutions of Zn^{II} tetrakis(N-methylpyridyl)porphyrin with Soret-band excitation: rapidly damped intermolecular modes with clustered solvent molecules and slowly damped intramolecular modes from the porphyrin macrocycle. *J. Phys. Chem. B* **2009**, *113*, 6127.

(20) Dillman, K. L.; Beck, W. F. Excited-state vibrational coherence in methanol solution of Zn^{II} tetrakis(N-methylpyridyl)porphyrin: charge-dependent intermolecular mode frequencies and implications for electron-transfer dynamics in photosynthetic reaction centers. *J. Phys. Chem. B* **2010**, *114*, 15269.

(21) Spence, T. G.; Trotter, B. T.; Burns, T. D.; Posey, L. A. Metal-to-ligand charge transfer in the gas-phase cluster limit. *J. Phys. Chem. A* **1998**, *102*, 6101.

(22) Vanderkooi, J. M.; Landesberg, R.; Hayden, G. W.; Owen, C. S. Metal-free and metal-substituted cytochromes *c*. Use in characterization of the cytochrome *c* binding site. *Eur. J. Biochem.* **1977**, *81*, 339.

(23) Ptitsyn, O. B. The molten globule state. In *Protein Folding*; Creighton, T. E., Ed.; W. H. Freeman and Co.: New York, 1993; p 243.

(24) Ohgushi, M.; Wada, A. "Molten-globule state": a compact form of globular proteins with mobile side-chains. *FEBS Lett.* **1983**, *164*, 21.

(25) Hamada, D.; Kuroda, Y.; Kataoka, M.; Aimoto, S.; Yoshimura, T.; Goto, Y. Role of heme axial ligands in the conformational stability of the native and molten globule states of horse cytochrome *c*. *J. Mol. Biol.* **1996**, *256*, 172.

(26) Anni, H.; Vanderkooi, J. M.; Mayne, L. Structure of zinc-substituted cytochrome *c*: nuclear magnetic resonance and optical spectroscopic studies. *Biochemistry* **1995**, *34*, 5744.

(27) Qian, C.; Yao, Y.; Tong, Y.; Wang, J.; Tang, W. Structural analysis of zinc-substituted cytochrome *c*. *J. Biol. Inorg. Chem.* **2003**, *8*, 394.

(28) Takano, T.; Dickerson, R. E. Redox conformation changes in refined tuna cytochrome *c*. *Proc. Natl. Acad. Sci. U.S.A.* **1980**, *77*, 6371.

(29) Teczan, F. A.; Crane, B. R.; Winkler, J. R.; Gray, H. B. Electron tunneling in protein crystals. *Proc. Natl. Acad. Sci. U.S.A.* **2001**, *98*, 5002.

(30) Goto, Y.; Calciano, L. J.; Fink, A. L. Acid-induced folding of proteins. *Proc. Natl. Acad. Sci. U.S.A.* **1990**, *87*, 573.

(31) Damaschun, G.; Gernat, C.; Damaschun, H.; Bychkova, V. E.; Ptitsyn, O. B. Comparison of intramolecular packing of a protein in native and "molten globule" states. *Int. J. Biol. Macromol.* **1986**, *8*, 226.

(32) Kataoka, M.; Hagihara, Y.; Mihara, K. i.; Goto, Y. Molten globule of cytochrome *c* studied by small angle X-ray scattering. *J. Mol. Biol.* **1993**, *229*, 591.

(33) Kamiyama, T.; Sadahide, Y.; Nogusa, Y.; Gekko, K. Polyol-induced molten globule of cytochrome *c*: an evidence for stabilization by hydrophobic interaction. *Biochim. Biophys. Acta* **1999**, *1434*, 44.

(34) Shibata, Y.; Takahashi, H.; Kaneko, R.; Kurita, A.; Kushida, T. Conformational fluctuation of native-like and molten-globule-like cytochrome *c* observed by time-resolved hole burning. *Biochemistry* **1999**, *38*, 1802.

(35) Lyubovitsky, J. G.; Gray, H. B.; Winkler, J. R. Structural features of the cytochrome *c* molten globule revealed by fluorescence energy transfer kinetics. *J. Am. Chem. Soc.* **2002**, *124*, 14840.

(36) Tremain, S. M.; Kostić, N. M. Molten-globule and other conformational forms of zinc cytochrome *c*. Effect of partial and complete unfolding of the protein on its electron-transfer reactivity. *Inorg. Chem.* **2002**, *41*, 3291.

(37) Bongiovanni, C.; Sinibaldi, F.; Ferri, T.; Santucci, R. Glycerol-induced formation of the molten globule from acid-denatured cytochrome *c*: implication for hierarchical folding. *J. Protein Chem.* **2002**, *21*, 35.

(38) Lampa-Pastirk, S.; Lafuente, R. C.; Beck, W. F. Excited-state axial-ligand photodissociation and nonpolar protein-matrix reorganization in Zn(II)-substituted cytochrome *c*. *J. Phys. Chem. B* **2004**, *108*, 12602.

(39) Lampa-Pastirk, S.; Beck, W. F. Polar solvation dynamics in Zn(II)-substituted cytochrome *c*: diffusive sampling of the energy landscape in the hydrophobic core and solvent-contact layer. *J. Phys. Chem. B* **2004**, *108*, 16288.

(40) Lampa-Pastirk, S.; Beck, W. F. Intramolecular vibrational preparation of the unfolding transition state of Zn^{II} substituted cytochrome *c*. *J. Phys. Chem. B* **2006**, *110*, 22971.

(41) Barns, K. J.; Lampa-Pastirk, S.; Dillman, K. L.; Beck, W. F. Intramolecular vibrational excitation of unfolding reactions in Zn^{II}-substituted and metal-free cytochromes *c*: activation enthalpies from integrated fluorescence Stokes shift and lineshape excitation profiles. *J. Phys. Chem. B* **2008**, *112*, 15108.

(42) Dixon, D. W.; Kirmaier, C.; Holten, D. Picosecond photodissociation of six-coordinate iron(II) porphyrins. *J. Am. Chem. Soc.* **1985**, *107*, 808.

(43) Rosca, F.; Kumar, A. T. N.; Ionascu, D.; Ye, X.; Demidov, A. A.; Sjodin, T.; Wharton, D.; Barrick, D.; Sligar, S. G.; Yonetani, T.; Champion, P. M. Investigations of anharmonic low-frequency oscillations in heme proteins. *J. Phys. Chem. A* **2002**, *106*, 3540.

(44) Bushnell, G. W.; Louie, G. V.; Brayer, G. D. High-resolution three-dimensional structure of horse heart cytochrome *c*. *J. Mol. Biol.* **1990**, *214*, 585.

(45) Bai, Y.; Sosnice, T. R.; Mayne, L.; Englander, S. W. Protein folding intermediates: native-state hydrogen exchange. *Science* **1995**, *269*, 192.

(46) Vanderkooi, J. M.; Adar, F.; Ericińska, M. Metallocytochromes *c*: characterization of electronic absorption and emission spectra of Sn^{4+} and Zn^{2+} cytochromes *c*. *Eur. J. Biochem.* **1976**, *64*, 381.

(47) Elias, H.; Chou, M. H.; Winkler, J. R. Electron-transfer kinetics of Zn-substituted cytochrome *c* and its $Ru(NH_3)_5$(Histidine-33) derivative. *J. Am. Chem. Soc.* **1988**, *110*, 429.

(48) Ye, S.; Shen, C.; Cotton, T. M.; Kostić, N. M. Characterization of zinc-substituted cytochrome *c* by circular dichroism and resonance Raman spectroscopic methods. *J. Inorg. Biochem.* **1997**, *65*, 219.

(49) Lakowicz, J. R. *Principles of Fluorescence Spectroscopy*, 2nd ed.; Kluwer Academic/Plenum Publishers: New York, 1999.

(50) Fragnito, H. L.; Bigot, J.-Y.; Becker, P. C.; Shank, C. V. Evolution of the vibronic absorption spectrum in a molecule following impulsive excitation with a 6-fs optical pulse. *Chem. Phys. Lett.* **1989**, *160*, 101.

(51) Schoenlein, R. W.; Peteanu, L. A.; Mathies, R. A.; Shank, C. V. The first step in vision: femtosecond isomerization of rhodopsin. *Science* **1991**, *254*, 412.

(52) Dexheimer, S. L.; Wang, Q.; Peteanu, L. A.; Pollard, W. T.; Mathies, R. A.; Shank, C. V. Femtosecond impulsive excitation of nonstationary vibrational states in bacteriorhodopsin. *Chem. Phys. Lett.* **1992**, *188*, 61.

(53) Pollard, W. T.; Mathies, R. A. Analysis of femtosecond dynamic absorption spectra of nonstationary states. *Annu. Rev. Phys. Chem.* **1992**, *43*, 497.

(54) Wang, Q.; Schoenlein, R. W.; Peteanu, L. A.; Mathies, R. A.; Shank, C. V. Vibrationally coherent photochemistry in the femtosecond primary event of vision. *Science* **1994**, *266*, 422.

(55) Zhu, L.; Sage, J. T.; Champion, P. M. Observation of coherent reaction dynamics in heme proteins. *Science* **1994**, *266*, 629.

(56) Wang, W.; Demidov, A.; Ye, X.; Christian, J. F.; Sjodin, T.; Champion, P. M. Application of femtosecond coherence spectroscopy to the observation of nuclear motions in heme proteins and transparent solutions. *J. Raman Spectrosc.* **2000**, *31*, 99.

(57) Rosca, F.; Kumar, A. T. N.; Ionascu, D.; Sjodin, T.; Demidov, A. A.; Champion, P. M. Wavelength selective modulation in femtosecond pump-probe spectroscopy and its application to heme proteins. *J. Chem. Phys.* **2001**, *114*, 10884.

(58) Cantor, C. R.; Schimmel, P. R. *Biophysical Chemistry. Part II: Techniques for the Study of Biological Structure and Function*; W. H. Freeman and Co.: San Francisco, 1980.

(59) McHale, J. L. *Molecular Spectroscopy*; Prentice Hall: Upper Saddle River, NJ, 1999.

(60) Cong, P.; Deuhl, H. P.; Simon, J. D. Using optical coherence to measure the ultrafast electronic dephasing of large molecules in room-temperature liquids. *Chem. Phys. Lett.* **1993**, *212*, 367.

(61) Joo, T.; Jia, Y.; Yu, J.-Y.; Lang, M. J.; Fleming, G. R. Third-order nonlinear time domain probes of solvation dynamics. *J. Chem. Phys.* **1996**, *104*, 6089.

(62) Xu, Q.-H.; Ma, Y.-Z.; Stiopkin, I. V.; Fleming, G. R. Wavelength-dependent resonant homodyne and heterodyne transient grating spectroscopy with a diffractive optics method: solvent effect on the third-order signal. *J. Chem. Phys.* **2002**, *116*, 9333.

(63) Rosca, F.; Kumar, A. T. N.; Ye, X.; Sjodin, T.; Demidov, A.; Champion, P. M. Investigations of coherent vibrational oscillations in myoglobin. *J. Phys. Chem. A* **2000**, *104*, 4280.

(64) Rosca, F.; Ionascu, D.; Kumar, A. T. N.; Demidov, A. A.; Champion, P. M. Femtosecond coherence spectroscopy using spectrally selective differential photodetection. *Chem. Phys. Lett.* **2001**, *337*, 107.

(65) Albrecht, A. C. "Forbidden" character in allowed electronic transitions. *J. Chem. Phys.* **1960**, *33*, 156.

(66) Tang, J.; Albrecht, A. C. Developments in the theories of vibrational Raman intensities. In *Raman Spectroscopy: Theory and Practice*; Szymanski, H. A., Ed.; Plenum: New York, 1970; Vol. 2, p 33.

(67) Walsh, A. M.; Loring, R. F. Theory of resonant and nonresonant impulsive stimulated Raman scattering. *Chem. Phys. Lett.* **1989**, *160*, 299.

(68) Pollard, W. T.; Fragnito, H. L.; Bigot, J.-Y.; Shank, C. V.; Mathies, R. A. Quantum-mechanical theory for 6 fs dynamic absorption spectroscopy and its application to nile blue. *Chem. Phys. Lett.* **1990**, *168*, 239.

(69) Pollard, W. T.; Lee, S.-Y.; Mathies, R. A. Wave packet theory of dynamic absorption spectra in femtosecond pump−probe experiments. *J. Chem. Phys.* **1990**, *92*, 4012.

(70) Carson, E. A.; Diffey, W. M.; Shelly, K. R.; Lampa-Pastirk, S.; Dillman, K. L.; Schleicher, J. M.; Beck, W. F. Dynamic-absorption

spectral contours: vibrational phase-dependent resolution of low-frequency coherent wave-packet motion of IR144 on the ground and excited $\pi \rightarrow \pi^*$ surfaces. *J. Phys. Chem. A* **2004**, *108*, 1489.

(71) Enescu, M.; Steenkeste, K.; Tfibel, F.; Fontaine-Aupart, M.-P. Femtosecond relaxation processes from upper excited states of tetrakis-(N-methyl-4-pyridyl)porphyrins studied by transient absorption spectroscopy. *Phys. Chem. Chem. Phys.* **2002**, *4*, 6092.

(72) Jean, J. M.; Fleming, G. R. Competition between energy and phase relaxation in electronic curve crossing processes. *J. Chem. Phys.* **1995**, *103*, 2092.

(73) Schrauben, J. N.; Dillman, K. L.; Beck, W. F.; McCusker, J. K. Vibrational coherence in the excited state dynamics of $Cr(acac)_3$: probing the reaction coordinate for ultrafast intersystem crossing. *Chem. Sci.* **2010**, *1*, 405.

(74) Vos, M. H.; Breton, J.; Martin, J. L. Electronic energy transfer within the hexamer cofactor system of bacterial reaction centers. *J. Phys. Chem. B* **1997**, *101*, 9820.

(75) Stanley, R. J.; King, B.; Boxer, S. G. Excited state energy transfer pathways in photosynthetic reaction centers. 1. Structural symmetry effects. *J. Phys. Chem.* **1996**, *100*, 12052.

(76) Spiro, T. G.; Kozlowski, P. M.; Zgierski, M. Z. New developments in the calculation of metalloporphyrin Raman spectra via density functional theory. *J. Raman Spectrosc.* **1998**, *29*, 869.

(77) Nappa, M.; Valentine, J. S. The influence of axial ligands on metalloporphyrin visible absorption spectra. Complexes of tetraphenylporphinatozinc. *J. Am. Chem. Soc.* **1978**, *100*, 5075.

(78) Humphry-Baker, R.; Kalyanasundaram, K. Influence of axial ligation on the fluorescence of tetrakisphenylporphyrins. *J. Photochem.* **1985**, *31*, 105.

(79) Vogel, G. C.; Beckmann, B. A. Binding of pyridine to phenyl-substituted derivatives of zinc tetraphenylporphine. *Inorg. Chem.* **1976**, *15*, 483.

(80) Scheidt, R. W. Porphyrin stereochemistry. In *The Porphyrins*; Dolphin, D., Ed.; Academic Press: New York, **1978**; Vol. 3, p 463.

(81) Fleischer, E. B.; Miller, C. K.; Webb, L. E. Crystal and molecular structures of some metal tetraphenylporphines. *J. Am. Chem. Soc.* **1964**, *86*, 2342.

(82) Schauer, C. K.; Anderson, O. P.; Eaton, S. S.; Eaton, G. R. Crystal and molecular structure of a six-coordinate zinc porphyrin: bis(tetrahydrofuran)(5,10,15,20-tetraphenylporphinato)zinc(II). *Inorg. Chem.* **1985**, *24*, 4082.

(83) Scheidt, R. W.; Eigenbrot, C. W.; Ogiso, M.; Hatano, K. Stereochemistry of a porphyrin atropisomer. The molecular and crystal structure of six-coordinate [5α,10β-bis(*o*-nicotinamidophenyl)-15,20-diphenylporphinato]zinc(II). *Bull. Chem. Soc. Jpn.* **1987**, *60*, 3529.

(84) Jordan, T.; Eads, J. C.; Spiro, T. G. Secondary and tertiary structure of the A-state of cytochrome *c* from resonance Raman spectroscopy. *Protein Sci.* **1995**, *4*, 716.

(85) London, F. The general theory of molecular forces. *Trans. Faraday Soc.* **1937**, *33*, 8.

(86) Margenau, H. Van der Waals forces. *Rev. Mod. Phys.* **1939**, *11*, 1.

(87) Kauzmann, W. *Quantum Chemistry: An Introduction*; Academic Press: New York, 1957.

(88) Berry, R. S.; Rice, S. A.; Ross, J. *Physical Chemistry*, 2nd ed.; Oxford University Press: New York, 2000.

(89) Berghuis, A. M.; Brayer, G. D. Oxidation state-dependent conformational changes in cytochrome *c*. *J. Mol. Biol.* **1992**, *223*, 959.

(90) Pielak, G. J.; Auld, D. S.; Betz, S. F.; Hilgen-Willis, S. E.; Garcia, L. L. Nuclear magnetic resonance studies of class I cytochromes *c*. In *Cytochrome c: a Multidisciplinary Approach*; Scott, R. A., Mauk, A. G., Eds.; University Science Books: Sausalito, CA, 1996, p 203.

(91) Deisenhofer, J.; Epp, O.; Miki, K.; Huber, R.; Michel, H. Structure of the protein subunits in the photosynthetic reaction center of *Rhodopseudomonas viridis* at 3.1 Å resolution. *Nature* **1985**, *318*, 618.

(92) Boxer, S. G.; Goldstein, R. A.; Lockhart, D. J.; Middendorf, T. R.; Takiff, L. Excited states, electron-transfer reactions, and intermediates in bacterial photosynthetic reaction centers. *J. Phys. Chem.* **1989**, *93*, 8280.

(93) Lubitz, W.; Lendzian, F.; Scheer, H.; Gottstein, J.; Plato, M.; Möbius, K. Structural studies of the primary donor cation radical P_{870}^+ in reaction centers of *Rhodospirillum rubrum* by electron-nuclear double resonance in solution. *Proc. Natl. Acad. Sci. U.S.A.* **1984**, *81*, 1401.